Formation, structure and magnetism of the $\gamma-$(Fe, M)$_{23}$C$_6$

(M= Cr, Ni) phases: a first-principles study

C.M. Fang[1], M.A. van Huis[1], M.H.F. Sluiter[2]

[1] *Soft Condensed Matter, Debye Institute for Nanomaterials Science, Utrecht University,*

Princetonplein 5, 3584 CC Utrecht, The Netherlands

[2]*Department of Materials Science and Engineering, Delft University of Technology, Mekelweg*

2, 2628 CD Delft, The Netherlands

1

Abstract

The γ-(Fe,M)$_{23}$C$_6$ phases constitute an important class of iron carbides. They occur both as precipitates in steels and iron alloys, thereby increasing their strength, and as common minerals in meteorites and in iron-rich parts of the Earth's mantle. Here we investigate the composition-dependent relative stability of these phases and the role of magnetism therein. The γ-(Fe,M)$_{23}$C$_6$ phases have mineral names isovite (M=Cr) and haxonite (M=Ni), and have a complex crystal structure (116 atoms in the cubic unit cell) in which the metal atoms have a rich variety of atomic coordination numbers, ranging from 12 to 16. First-principles calculations show a narrow formation range for γ-(Fe$_{1-x}$Ni$_x$)$_{23}$C$_6$ (x ~ 0.043), while the formation range for γ-(Fe$_{1-x}$Cr$_x$)$_{23}$C$_6$ is very broad with x = 0 to 0.85 and x ~ 0.91, in good agreement with available experimental data. The present study also shows the importance of magnetism on the formation and stability of these compounds. The conditions of formation and several factors enhancing or hampering the formation of γ-(Fe,M)$_{23}$C$_6$ in man-made steels and in meteorites are discussed.

I. Introduction

Since the discovery of γ-$Cr_{23}C_6$ by Westgren [1], this cubic phase has been reported in many steels [2-6]. Recently Jin and co-workers found γ-$(Fe,M)_{23}C_6$ nano-particles (with radii of 4 to 8 nm) at dislocation loops of ion-irradiated austenitic steels [7]. Taneike and co-workers also revealed that nano-sized precipitates play a crucial role in the physical properties of steels [8]. This shows the importance of understanding the formation and stability of these precipitates in metallurgy and for the development of new steels [7-14]. In addition, these compounds are also earth materials. The γ-$(Fe,Cr)_{23}C_6$ phase occurs in the lower mantle of the earth and is then referred to as the mineral isovite [15,16], whereas the haxonite phase γ-$(Fe,Ni)_{23}C_6$ containing about 4.9 at% Ni was discovered by Scott in the 1970s [17]. Haxonite was subsequently observed in many iron meteorites [17-22]. Information on the formation, stability and physical properties of these minerals is very helpful for planetary researchers and geophysicists to understand the history of meteorites, and to understand the formation of minerals in the Earth's mantle [18-23].

The γ-$(Fe,M)_{23}C_6$ phases exhibits a rich variety in crystal chemistry. There are 4 crystallographically distinct species of metal sites that have coordination numbers varying from 12 to 16 [1-4, 17,23]. The carbon atoms in this cubic phase are also uniquely coordinated by 8 metals atoms (Figure 1), in contrast to those in most metal carbides, where C atoms are octahedrally coordinated [1,2,10,13,14]. The chemical compositions of isovite and haxonite as observed in meteorites are quite unusual in metallurgy. γ-$(Fe,Cr)_{23}C_6$ was found in many Cr-containing steels with a wide range of Cr/Fe ratios at elevated temperatures [24,25], while γ-$(Fe,Ni)_{23}C_6$ was only discovered in iron meteorites with about 4.9 at% Ni [17-22], and to date there are no reports on γ-$(Fe,Ni)_{23}C_6$ phases observed in steels or alloys [2,14,26].

The phase diagrams of the ternary Fe-Cr-C system show that γ-(Fe,Cr)$_{23}$C$_6$ has a Fe/Cr alloying range from 0.0 % to ~88 mass% of Fe at elevated temperature [24,25], while experimental studies for Fe-Ni-C systems showed stable Fe-Ni alloys, but only metastable carbides [27,28]. There are no observations of the cubic γ-(Fe,Ni)$_{23}$C$_6$ phase in steels [14,27-30].

Theoretical efforts have been made for the γ-M$_{23}$C$_6$ phases and related compounds in the Fe-M-C system, but mainly on binary carbides [11,12,31-42]. Using a pair-potential approach, Xie and co-workers explored a series of γ-(Cr, M)$_{23}$C$_6$ (M=Fe, W, Ni) compounds in detail [11,12]. However, the absence of magnetic effects in these calculations is a serious shortcoming. Jiang [31] and Widom, *et al.*[32,33] investigated the compounds in the binary Cr-C system using a first-principles approach and found a high stability for the γ-Cr$_{23}$C$_6$ phase. Wallenius and co-workers investigated binary carbides including γ-M$_{23}$C$_6$ (M=Cr or Fe) and a mixed Cr$_{22}$FeC$_6$ phase in the Fe-Cr-C system [34]. Dos Santos *et al.* explored the magnetism of γ-Cr$_{23}$C$_6$ using the linear muffin-tin orbital (LMTO) approach with Andersen's atomic sphere approximation (ASA) with local spin approximation (LSDA) and also with the linearized augmented plane wave (LAPW) method with a generalized gradient approximation (GGA) exchange-correlation potential, and obtained small magnetic moments for the Cr atoms at the Wyckoff 4a sites [35]. Many first-principles calculations have been applied to iron carbides as well [36,37,39-42]. Recently a systematic first-principles study on the stability of binary Fe-C compounds revealed that although being meta-stable with respect to the elemental solids (ferrite and graphite), γ-Fe$_{23}$C$_6$ is slightly more stable than the well-known cementite phase, θ-Fe$_3$C [39,40]. Both theoretical calculations and experimental observations agreed that during the thermal treatments of Fe-C alloys, the hexagonal close packed (hcp) family phases (ε-Fe$_2$C, η-Fe$_2$C, χ-Fe$_5$C$_2$, and θ-Fe$_3$C) are formed while there is

no trace of formation of γ-$Fe_{23}C_6$ [2,37-44]. This is due to the unique crystal structure of γ-$Fe_{23}C_6$ [13,39]. To date no reliable theoretical calculations have been performed for γ-$(Fe,Ni)_{23}C_6$ phases.

In this paper, we present a systematic study on the γ-$(Fe,M)_{23}C_6$ (M = Cr, Ni) phases using the density functional theory (DFT) within the generalized gradient approximation (GGA). The calculated formation energies are compared with the cohesive energies of 3d transition metal carbides obtained by Guillermet and Grimvall [45]. We obtained a broad formation range for M=Cr and a very narrow range for M = Ni in agreement with the available experimental observations [1-4,17-20,24-30]. The local chemical bonding and the electronic and magnetic properties are addressed and discussed in relation to stability. The information obtained here is useful to understand the formation, occurrence, and characterization of the γ-$(Fe,Ni)_{23}C_6$ and γ-$(Fe,Cr)_{23}C_6$ phases in different steels and alloys (metallurgy) and in both iron meteorites and the Earth's mantle (geosciences).

II. Details of theoretical calculations

A. Formation energy

The formation energy is used to assess the relative stability of the compound relative to the elemental solids. The formation energy (ΔE, per atom) for a ternary carbide ($M_nM'_{n'}C_m$) is defined from the pure solids of the elemental phases (M =α-Fe, M'=α-Cr or $\gamma-$Ni, and graphite) [13,35-42,46]:

$$\Delta E = \{E(M_nM'_{n'}C_m) - [n\,E(M) + n'\,E(M') + m\,E(C)]\}/(n+n'+m) \tag{1}$$

At a temperature of $T = 0$ K and a pressure of $P = 0$ Pa, the formation enthalpy is equal to the formation energy, i.e. $\Delta H(M'_{n'}M_nC_m) = \Delta E(M'_{n'}M_nC_m)$, when the zero-point vibration contribution is ignored.

We considered different Fe/M (M=Cr,Ni) alloying ratios in γ-$(Fe,M)_{23}C_6$, while retaining the symmetry of the cubic phases. As shown before, magnetic ordering plays an important role in 3d transition metal compounds [31-44,46-48]. As shown in Figure 1, there are 4 crystallographically different types of metal atoms. Using the Heisenberg-Ising model, there will be eight different magnetic arrangements, $(M1)\uparrow(M2)\uparrow\downarrow(M3)\uparrow\downarrow(M4)\uparrow\downarrow$. Naturally, each metal atom/ion may exhibit a high-spin (HS) or a low-spin (LS) solution. So for each composition, there will be 64 possible magnetic configurations. Fortunately, we can reduce the numbers by considering the facts that most Fe/Ni compounds including carbides are ferromagnetic (FM) or ferrimagnetic (FRM) [31-44,46-48]. Therefore, the ferromagnetic or ferrimagnetic ordering was taken as starting for the Fe/Ni carbides. Meanwhile, possibilities of other magnetic configurations were taken into account as well. For Fe/Cr carbides, we performed calculations for the 8 configurations for each chemical composition with extra consideration of the spin-states. The calculations showed that most of the different inputs were converged to one solution for the Ni/Fe systems. For the Fe/Cr carbides, we obtained multiple magnetic configurations among which we present the most stable ones only in the section below.

B. Crystal structure of γ-$M_{23}C_6$

In 1933 Westgren reported the crystal structure of γ-$Cr_{23}C_6$ [1]. This representative of the cubic γ-$M_{23}C_6$ phase has space group $Fm\overline{3}m$ (nr. 225) [1-3,11-14,39]. There are four

crystallographically distinct kinds of M atoms in γ-$M_{23}C_6$: M1 at the Wyckoff sites 4a, M2 at 8c, M3 at 32f and M4 at 48h, as shown in Figure 1. Therefore, we can present the formula as $(M1)_1(M2)_2(M3)_8(M4)_{12}C_6$ according to its structural characterization. Careful analysis reveals that this crystal structure can be considered as composed of two parts: a framework containing sets of strongly linked M-sublattices (M3 and M4), additional stabilizing metal atoms (M1 and M2), and C atoms positioned in cavities of the framework. The coordination of M and C atoms in the γ-$M_{23}C_6$ phases varies strongly: Each M1 atom has 12 M4 nearest neighbors; each M2 has only 4 M3 nearest neighbors and 12 M4 atoms with a greater distance in the range of 2.7 to 2.9 Å. Both M3 and M4 have 10 M nearest neighbors and 2 or 3 C neighbors. The C atoms have eight M nearest neighbors. Such a coordination of the C atoms is unusual, since most C atoms are octahedrally coordinated in the transition metal carbides [1-4,12-16,39].

In the present calculations, we mostly retain the crystal symmetries. We also performed calculations for selected cases with broken symmetries, e.g. replacing one Fe at one of the M1, M2, M3, or M4 sites by Ni/Cr in the γ-$Fe_{23}C_6$ phase in order to find the preferred site for the Ni/Cr atom.

C. Computational settings

For all calculations, the code VASP (Vienna *Ab initio* Simulation Package version 4.6.34)[49-51] which uses the density functional theory (DFT) within the Projector-Augmented Wave (PAW) method was employed [52,53]. The (spin-polarized) generalized gradient approximation (GGA) formulated by Perdew, Burke, and Ernzerhof (PBE) [54] was employed for the exchange and correlation energy terms, since it has proved that the GGA

approximation describes spin-polarized 3d transition metals better than the local- (spin-polarized) density approximation (LDA) [39,55]. The cut-off energy of the wave functions was 500 eV. The cut-off energy of the augmentation functions was about 645 eV. The integrations in reciprocal space were performed on a $12\times12\times12$ grid with 72 k-points, in the irreducible Brillouin zone (BZ) of γ-$M_{23}C_6$, using the Monkhorst and Pack method [56], while a $24\times24\times24$ grid with 364 k-points was used in the irreducible Brillouin zones (BZ) of α-Fe, α-Cr, $\gamma-$Ni and C in the diamond structure. Structural optimizations were performed for both lattice parameters and coordinates of atoms. For the calculations of local electronic configurations and partial density of states of atoms, the Wigner-Seitz radius is set at 1.4 Å for Fe/Ni and 1.0 Å for C, respectively. Note that Fe/Ni 4s, 4p and 3d electrons and C 2s, 2p electrons exhibit an itinerant character in alloys and carbides and in principle belong to the whole crystal. However, we can decompose the plane waves in the sphere and obtain e.g. the Fe/Ni 3d components in the spheres for both spin-up (or majority) and spin-down (minority) direction. In this way a local magnetic moment is obtained that is the difference of the spin-up electrons and spin-down electrons in the sphere. In the calculations for γ-$(Fe,M)_{23}C_6$ phases, for M = Ni ferromagnetic ordering was used as initial guess, while for M = Cr, several additional antiferromagnetic orderings used as initial guesses in order to obtain the most stable magnetic configurations. Various k-meshes were tested, e.g. $8\times8\times8$ (29 k-points) to $16\times16\times16$ (142 k-points) grids for γ-$M_{23}C_6$, as well as cut-off energies for the waves and augmentation waves, respectively. The tests of k-mesh and cut-off energies showed a good convergence (~ 1 meV/atom).

III. Calculated results

A. Elemental metals (Cr, Fe and Ni)

The ground states of the 3d transition metal series have been a topic of intensive investigations [53,55-61]. The ferromagnetism has been well-established for body-centered cubic (α-)Fe and for face-centered cubic (γ-)Ni [57,58]. Meanwhile, the magnetic structure of the ground-state of Cr has been debated [59-62]. At the ground state, Cr has a body-centered structure (α). Early work proposed that α-Cr has a spin-density-wave (SDW) structure [59]. Accurate calculations find difficulties to confirm the SDW model [60,61]. Recent first-principles calculations indicate that the anti-ferromagnetic (AFM) ordering has a rather high-stability for α-Cr.[59-62] In the present work we therefore adopt the AFM model [60,61]. Our calculations give the lattice parameter and magnetic moment for AFM α-Cr that are very close to those by Cottenier and co-workers using high-precision full-potential linearized augmented plane wave within the generalized gradient approximation [61], as shown in Table 1. We also tested and calculated the structure and properties of face-centered cubic (fcc) Cr with different magnetic orderings as input configurations. All calculations resulted in the non-magnetic solution (NM). The calculated results for the ground states of α-Fe, α-Cr and γ-Ni are listed and compared with experiments in Table 1. It is generally known that carbon exhibits at least two phases, graphite and diamond. The ground state of carbon is graphite. Experiments have determined that at zero pressure and zero K, graphite is about 17 meV/atom more stable than diamond [39,40]. Therefore, we performed calculations for diamond and added a correction term in order to obtain the enthalpy for graphite. The calculated diamond lattice parameter is 3.5713 Å with details described in former publications [13,39-41]. As shown in Table 1, the present calculations for the 3d metals reproduce the experimental values as well as the former theoretical results.

B. Binary carbides γ-M$_{23}$C$_6$, (M=Cr, Fe and Ni)

Table 1 also lists the calculated results for binary γ-M$_{23}$C$_6$, including comparisons with experimental measurements and previous theoretical results. Structural information is experimentally available only for M = Cr [1-3]. Branagan and co-workers observed γ-M$_{23}$C$_6$ with M = Fe from crystallites formed during crystallization of amorphous alloys [63]. There is no report on γ-M$_{23}$C$_6$ with M=Ni. The calculated formation energies are in good agreement with the former calculations for M = Cr [31-33] and M = Fe [13,39,40]. Experimental phase stabilities also agree well with our calculations, showing high stability for γ-Cr$_{23}$C$_6$, meta-stability for γ-Fe$_{23}$C$_6$, and low stability for γ-Ni$_{23}$C$_6$ (Table 1). Our calculated formation energy for γ-Cr$_{23}$C$_6$ is close to that by Jiang,[31] but slightly different from those by Wallenius and co-workers who employed different cut-off energies for metals and carbides [32-34]. The energy difference caused by various cut-off energies in calculations is even more apparent for γ-Fe$_{23}$C$_6$ (Table 1). Guillermet and Grimvall studied the cohesive energies of 3d-transition metal carbides, including the γ-M$_{23}$C$_6$ phase [45]. As shown in Table 1, the calculated formation energies in the present work showed a stable phase for M = Cr, while the phases with M=Fe and M=Ni are metastable. The relative order of stability is: γ-Cr$_{23}$C$_6$ > γ-Fe$_{23}$C$_6$ > γ-Ni$_{23}$C$_6$, in line with the former analysis by Guillermet and Grimvall who calculated the value from experimental data on γ-Cr$_{23}$C$_6$ [45,64]. But for metastable γ-Fe$_{23}$C$_6$ and γ-Ni$_{23}$C$_6$, they estimated the values from interpolation and extrapolation procedures, assuming that the bonding properties vary smoothly as a function of the average number of valence electrons per atom in the compounds [45].

Our calculations reveal a rich variety of local magnetic moments for the γ-M$_{23}$C$_6$ phases as shown in Table 2. It is notable that in γ-Fe$_{23}$C$_6$ the local moment is about 2.82 μ_B in the sphere

of an Fe2 atom which has only 4 nearest neighbors (aside from another 12 neighbors at greater distance of about 2.88 Å). This agrees with the general rule that a lower coordination can increase local magnetic moments, e.g. Fe at surfaces [65,66]. The local moments for atoms in γ-$Ni_{23}C_6$ are small (with an average value of 0.06 μ_B) in comparison to that in γ-Ni (0.62 μ_B) (Table 1). This indicates that the present γ-$Ni_{23}C_6$ structure reduces the magnetism of Ni atoms. This phenomenon is not unusual as shown in our earlier work where it was found that for both fcc-Ni and hexagonally-close-packed (hcp-) Ni, addition of C reduces the magnetism [47,48]. The calculations also showed a high formation energy for this compound. The present calculations with various initial magnetic structures also resulted in the non-spin-polarized (or non-magnetic, NM) solution for γ-$Cr_{23}C_6$. This agrees with most of the former theoretical works [31-33], but it differs from the work by Dos Santos *et al.*[35], which is reasonable since our calculations for fcc-Cr also result in a non-magnetic solution at the ground state whereby γ-$Cr_{23}C_6$ has a defective fcc-Cr sublattice [1,13]. The small local magnetic moments for γ-$Cr_{23}C_6$ obtained by Dos Santos and co-workers may originate from the Atomic Spherical Wave (ASA) approximation [35].

We note that though it is widely accepted the larger local magnetic moment is related to the coordination numbers (CN), this idea has no solid physical basis as: a) as function of lattice parameter (or atomic volume) M of any magnetic element changes, while CN remains the same; 2) at low CN one expects not metallic but covalent and ionic bonding – which would quench the magnetic moment completely, e.g. a four-fold coordinated Fe would almost certainly NOT be magnetic. Therefore, we relate the local magnetic moment to its atomic volume. Using the Bader's approach which defines the boundary of an atom in a solid by the zero-flux surfaces between the atom and neighboring atoms [67], we obtained the Bader atomic volumes for γ-$Fe_{23}C_6$. Figure 2 shows the relationship between the atomic volume and

local magnetic moment in the spheres of Fe in γ-Fe$_{23}$C$_6$. Clearly the local magnetic moments of Fe increase with the atomic volumes.

As shown in Table 2, there is a trend that the number of electrons in the spheres of the metal atoms of the same kind slightly increases in the order: Cr (4.30 to 4.50 electrons) to Fe (6.30 to 6.65 electrons) to Ni (8.47 to 8.66 electrons) , while the number of electrons in the C spheres decreases (Table 2). That is due to (1) the increasing atomic number of the metal atoms from Cr, Fe to Ni, (2) the Pauli electronegativity of these elements (1.66 for Cr, 1.83 for Fe and 1.91 for Ni, vs. 2.55 for C). The smaller electronegativity difference between the metal to carbon indicates smaller charge transfer [47].

C. Formation energies and magnetism of ternary carbides γ-(Fe,M)$_{23}$C$_6$ (M = Ni, Cr)

We first performed calculations for the simple case where one metal atom in the binary γ-M$_{23}$C$_6$ (M =Fe, Ni, Cr) is replaced by another metal atom for the various Wyckoff sites. The results are shown in Table 3.

It is clear that, except for γ-Ni$_{22}$FeC$_6$, all phases with the foreign M at M1 have low formation energy. However for γ-Ni$_{22}$FeC$_6$, the configuration with Fe at one of the M2 sites is the most stable configuration. The magnetism for these γ-M$_{22}$M'C$_6$ phases is also complicated. γ-Cr$_{22}$FeC$_6$ is non-magnetic (NM). γ-Ni$_{22}$FeC$_6$ and γ-Fe$_{22}$NiC$_6$ are ferrimagnetic and the order of decreasing values of local magnetic moments is: M(M2, CN=4+12) > M(M1, CN=12)/and M(M3, CN=9+2) > M(M4, CN = 10 +3), here the first number of the coordination number of neighbors (CN) represents metal-metal coordination and the second metal-carbon coordination. Considering the reducing effects of C atoms, this order is consistent with the order of increasing CN numbers, as shown in Table 2. The Cr impurity in γ-Fe$_{22}$NiC$_6$ is

calculated to behave differently. All of them are antiferrimagnetic (AFRM) in the Fe frames. The local moment of Cr at the M2 site is smaller than that at the M1 site.

Our calculations showed that most of the γ-(Fe,Ni)$_{23}$C$_6$ phases have multiple ferrimagnetic solutions depending on magnetic starting configurations while some phases appear to have only a single stable magnetic configuration The calculations also show that most of the γ-(Fe,Cr)$_{23}$C$_6$ (Cr concentration > 35 atom %) phases are sensitive to the magnetic starting configuration. Therefore, for each phase we have to test several magnetic orderings to obtain solutions of the lowest formation energies. Figure 3 shows the formation energies for the most stable ternary γ-(Fe,Ni)$_{23}$C$_6$ and γ-(Fe,Cr)$_{23}$C$_6$ phases (top) along with their calculated lattice parameters (bottom). The local magnetic moments in the spheres of 3d metals are shown in Figure 4 for γ-(Fe,Ni)$_{23}$C$_6$ (top) and for γ-(Fe,Cr)$_{23}$C$_6$ (bottom).

As shown in Figure 3 (bottom), the lattice parameters of γ-(Fe$_{1-x}$M$_x$)$_{23}$C$_6$ vary in a small range (10.35 to 10.54 Å). As shown in Figure 3 and Table 1, the lattice parameters of binary γ-M$_{23}$C$_6$ decrease in the order Cr-Fe-Ni, in agreement with the order of decreasing atomic radii: Cr(1.66 Å), Fe (1.56 Å), and Ni (1.49 Å) [68]. With increasing Fe concentrations, the lattice parameter of the Cr-rich phases of the γ-(Fe$_x$Cr$_{1-x}$)$_{23}$C$_6$ system decreases, while it increases for the Ni-rich γ-(Fe$_x$Ni$_{1-x}$)$_{23}$C$_6$ phase.

Figure 3 (top) shows the calculated formation energies for the γ-(Fe$_{1-x}$M$_x$)$_{23}$C$_6$ phases. It is very clear that for most Ni-rich phases the formation energy is very high. There are only two compositions with formation energies lower than that of pure γ-Fe$_{23}$C$_6$. γ-Fe$_{22}$NiC$_6$ with Ni at the 4a sites has the lowest formation energy, ΔE ~5 meV/atom. Another phase with high stability is γ-Fe$_{20}$Ni$_3$C$_6$ with Ni at the 4a (M1) and 8c (M2) sites (ΔE ~ 18 m eV/atom). As shown in Figure 4 (top), the magnetic moments for Ni atoms are small (typically less than 0.9 μ_B) while Fe atoms have large moments (1.5 to 3.2 μ_B). The calculations show ferro-

magnetism for the γ-$(Fe_{1-x}Ni_x)_{23}C_6$ phases with two exceptions. One exception is the Fe1 atom in γ-$Fe_{15}Ni_8C_6$ that has a large moment of about 2.47 μ_B, but in an anti-ferromagnetic (AF) configuration in contrast to the other metal atoms. The second exception is γ-$Fe_{21}Ni_2C_6$, in which the Fe1 atoms have a small magnetic moment of about 0.2 μ_B, with an AF magnetic ordering in contrast to the other metal atoms. In both cases the formation energies are very high (>50 meV/atom).

The formation energies for the γ-$(Fe_xCr_{1-x})_{23}C_6$ phases are even more complex. However, analysis reveals that four different regions for the spin polarizations of Cr/Fe atoms can be distinguished, the Cr-rich part (R-Cr) with $x(Fe)$ <0.35, the Fe-rich part (R-Fe) with $x(Fe)$ >0.65 and two middle regions, R-M1 with Fe atoms occupying M3 sites ($x(Fe)$ = 0.61 to 0.54), and R-M2 with Fe occupying M4 sites ($x(Fe)$ = 0.65 to 0.52). For R-Cr, γ-$Cr_{22}FeC_6$ with Fe at the 4a (M1) has the lowest formation energy in the whole system. Another composition with reasonably high stability is γ-$Cr_{20}Fe_3C_6$ with Fe at the 4a (M1) and 8c (M2) sites. It is also notable that the Cr-rich phases ($x(Fe)$ <35 at.%) are non-magnetic, which is due to the magnetism-quenching effects of fcc-Cr [31]. For the phases in the R-M1 range, there is a magnetic transition. γ-$Cr_{14}Fe_9C_6$ becomes magnetic with Fe occupying both M1 and M3 sites (moments: M(Fe3) ~0.1 μ_B and M(Fe1) ~2.2 μ_B). γ-$Cr_{13}Fe_{10}C_6$ with Cr at the M1 sites becomes magnetic with a sizable moment -1.18 μ_B, which is comparable to that of α-Cr (see Table 1), while the Fe3 and Cr4 atoms have very small moments. As Fe atoms occupy the M4 sites (R-M2), magnetic moments of Fe atoms become comparable to those of pure γ-$Fe_{23}C_6$, as shown in Figure 4. Furthermore, γ-$Fe_{21}Cr_2C_6$ is calculated to be more stable than γ-$Fe_{23}C_6$ (Figure 3) with both the Cr at 8c and Fe1 at 4a sites are magnetically anti-parallel to those of other Fe atoms. All of the Fe-rich phases, except pure Fe phase are ferrimagnetic. The Cr atoms at M1 and M2 sites for the three compositions, γ-$Fe_{22}CrC_6$, γ-$Fe_{21}Cr_2C_6$ and γ-

Fe$_{20}$Cr$_3$C$_6$, have magnetic moments of about 2.1 to 2.4 μ_B with their orientation anti-parallel to that of the Fe atoms, which have magnetic moments similar to that of γ-Fe$_{23}$C$_6$, but which slightly decrease with increasing Cr concentration. Finally, there are four configurations with formation energies lower than the corresponding linear combinations of the binaries. These are γ-Fe$_{21}$Cr$_2$C$_6$, in the R-Fe range, γ-Fe$_{14}$Cr$_{10}$C$_6$ in the R-M2 range, γ-Cr$_{20}$Fe$_3$C$_6$ and γ-Cr$_{22}$Fe$_1$C$_6$ in the R-Cr range.

IV. Discussions: formation of haxonite in meteorites and isovite in steels

Our first-principles calculations for the γ-(Fe,M)$_{23}$C$_6$ phases at the ground states showed significant differences between M = Ni and Cr on stability, formation range and magnetic properties. The calculations showed a narrow formation region for γ-(Fe, Ni)$_{23}$C$_6$ phases. That is, high stability of Fe-rich γ-Fe$_{22}$NiC$_6$ with a formation energy about 5 meV/atom. In this phase the Ni content is about 4.3 at. % (or 4.6 wt %), which agrees well with the experimental observation (x(Ni) ~ 4.9 at. % or 5.2 wt % of the metals) [17].

γ-Fe$_{22}$NiC$_6$ has never been obtained in any man-made steels and alloys, in spite of its relatively high stability with a formation energy lower that of the well-known cementite phase at the ground state. However, this phase was observed in meteorites and may be present in the Earth mantle as well [17-21. The origin of iron meteorites has been under much discussion [18,74]. Iron meteorites are core fragments from differentiated and subsequently disrupted planetesimals. The parent bodies are usually assumed to have formed in the main asteroid belt, which is the source of most meteorites. The iron-meteorite parent bodies most probably formed in the terrestrial planet region. The time of formation of the iron meteorites is expected to be similar to that of our Earth. The large size of the iron meteorites (~hundreds of

meters) caused the cooling rate being much lower than what can be achieved in man-made Fe-C alloys/steels. Under cooling rates achievable in the laboratory other transformations take place; the formation of bcc Fe-rich kamacite, retained Ni-rich austenite taenite, and carbon expulsion through Fe-carbide formation (such as cohenite) through phase separation from the high temperature austenite phase. C atoms do not remain in the retained austenite phase because the high Ni concentration is unfavorable for C dissolution. Very slow cooling allows another avenue of C expulsion: formation of γ-$M_{23}C_6$ which might nucleate at GBs of the bcc-metal domains. As is apparent from our *ab initio* calculations the $M_{23}C_6$ phase is most stable when Ni atoms occupy the 4a sites only and exclusively. Hence a high degree of order on the M sublattices is required. Furthermore, as the comparison of $M_{23}C_6$ and a matching 3x3x3 fcc cell indicates, a large number of vacant M sites need to be present in the austenite phase before the $M_{23}C_6$ phase can replace the fcc phase. This suggests that the formation of $M_{23}C_6$ from austenite requires a large influx of vacancies that can occur only if the transformation progresses very slowly, such as under very slow cooling rates. In alloys with large B concentrations $M_{23}(C,B)_6$ may form relative easily as an intermediate phase that decomposes into more stable compounds as the temperature is lowered further [75]. In contrast, haxonite remains stable. The reason may be that in haxonite both Ni and C have already optimal local environments: Ni in a 12-fold Fe coordinated site without any C neighbors, and C at a well hybridized position involving 8 Fe nearest neighbors. Neither Ni nor C gains much from segregating to a Ni-rich austenite (taenite) or Fe-rich cementite (cohenite) phase, so that the $Fe_{22}NiC_6$ remains stable even as the temperature is lowered.

Our calculations show that the γ-$(Fe,Cr)_{23}C_6$ phase has a broad range of formation. Therefore, we expect complex formation ranges of isovite phases in the Cr-Fe-C phase diagram. However, in the Fe-rich range there is a strong competition between γ-$(Fe, Cr)_{23}C_6$ and some

hcp family members, such as $(Fe, Cr)_7C_3$, $(Fe, Cr)_3$, *etc.* that are relatively stable phases [31-33]. As shown in our earlier work [39-41], it is expected that the complex magnetic properties of the (Fe, Cr) carbides will play an important role in determining the relative stability of these related phases at elevated temperatures. Further investigations are required to better understand the relative stability.

V. Conclusions

The first-principles calculations predict broad and complex Cr/Fe alloying ranges in the γ-(Fe, Cr)$_{23}$C$_6$ phases, but a narrow Ni/Fe composition range for γ-(Fe,Ni)$_{23}$C$_6$, in good agreement with the experimental observations. Both the Cr and Ni containing phases exhibit very diverse magnetic properties, dependent on the specific composition. The high stability of γ-(Fe,Cr)$_{23}$C$_6$ indicates that these compounds can easily be formed as precipitates in steels. The metastability of γ-(Fe,Ni)$_{23}$C$_6$ in combination with its austenitic metal framework, explains that this phase is formed under very special conditions, such as in slow-cooling meteorites.

Acknowledgments

References

1. A. Westgren, Nature (London) 132, 480 (1933).

2. H. J. Goldschmidt, Nature (London) 162, 855 (1948).

3. J. F. Brown and D. Clare, Nature (London) 167, 728 (1951).

4. F.J. Radd and L. H. Crowder, Nature (London) 181, 258(1958).

5. B. E. Hopkinson and K. G. Carroll, Nature (London) 184, 1479(1959).

6. H. Letner, M. Bishof, H. Clemens, S. Erlach, B. Sonderegger, E. Kozeschnik, J. Svoboda and F. D. Fischer, Adv. Engin. Mater. 8, 1066(2006).

7. S. X. Jin, L. P. Guo, F. F. Luo, Z.W. Yao, S. L. Ma and R. Tang, Scripta Mater. 68, 138 (2013).

8. M. Taneike, F. Abe and K. Sawada, Nature (London) 424, 294 (2003).

9. M. M. Serna, E. R. B. Jesus, E. Galego, L. G. Martinez, H. P. S. Corrêa, and J. L. Rossi, Mater. Sci. Forum 530-531, 48(2006).

10. G. K. Tirumalasetty, M. A. van Huis, C. M. Fang, Q. Xu, F. D. Tichelaar, D. N. Hanlon, J. Sietsma and H. W. Zandbergen, Acta Mater. 59, 7406 (2011).

11. J. Y. Xie, N. X. Chen, J. Shen, L. D. Teng and S. Seetharaman, Acta Mater. 53, 2727 (2005).

12. J. Y. Xie, J. Shen, N. X. Chen and S. Seetharaman Acta Mater. 54,4653 (2006).

13. C. M. Fang, M. A. van Huis, and H. W. Zandbergen, Comp. Mater. Sci.51, 146 (2012).

14. S. Nagakura and S. Oketani, Transactions ISIJ 8, 265 (1968).

15. F. V. Kaminsky and R. Wirth, Canadian Mineralogist 49, 555 (2011).

16. F. V. Kaminsky, Earth Sci. Rev. 110, 127(2012).

17. E. R. D. Scott, Nature (London) 229, 61 (1971).

18. H. A. Axon, Progr. Mater. Sci. 13, 183 (1968).

19. R. Brett, Science 153, 60(1966).

20. E. R. D. Scott and J. T. Wasson, Rev. Geophys. Space Phys. 13, 527 (1975).

21. E. R. D. Scott, and R. H. Jones, Geochim. Cosmochim. Acta 54, 2485 (1990).

22. J. M. Knudsen, Hyperfine Interactions 47, 13(1989).

23. A. L. Bowman, G. D. Arnold, E. K. Storms and N. G. Nereson, Acta Crystallogr. B28, 3102 (1972).

24. V. Raghavan, J. Phase Equilibria 23, 513 (2002).

25. S. Atamert and H. K. D. H. Bhadeshia, Mater. Sci. Engin. A130. 101 (1990).

26. A. D. Romig, Jr. and J. I. Goldstein, Metallurg. Transact. A9, 1599 (1978).

27. K. B. Reuter, D. B. Williams and J. I. Goldstein, Metallurg. Transac. A20, 719 (1989).

28. V. Raghavan, J. Phase Equilibria 15, 428 (1994).

29. A. M. Sherman, G. T. Eldis and M. Cohen, Metallurg. Transact. A14, 995 (1983).

30. T. N. Durlu, J. Mater. Sci. Lett. 15, 1510 (1996).

31. C. Jiang, Appl. Phys. Lett. 92, 041090 (2008).

32. M. Widom and M. Mihalkovic, J. Mater. Resch. 20, 237 (2005).

33. P.R. Ohodnicki, N. C. Cates, D. E. Laughlin, M. E. McHenry and M. Widom, Phys. Rev. B78, 144414 (2008).

34. J. Wallenius, N. Sandberg and K. Henriksson, J. Nucl. Mater. 415, 316 (2011).

35. A. V. dos Santos, Physica B 387, 136 (2007).

36. Y. F. Li, Y. M. Gao, B. Xiao, T. M., Y. Yang, S. Q. Ma and D. W. Yi, J. Alloys and Compounds 509, 5242 (2011).

37. H. I. Faraoun, Y. D. Zhang, C. Esling and H. Aourag, J. Appl. Phys.99,093508 (2006).

38. J. Häglund and A. F. Guillermet, Phys. Rev. B48, 11685 (1993).

39. C.M. Fang, M.A. van Huis, M.H.F. Sluiter, H.W. Zandbergen, Acta Mater.58, 2968 (2010).

40. C.M. Fang, M.H.F. Sluiter, M.A. van Huis, C. K. Ande, and H.W. Zandbergen, Phys. Rev. Lett. 105, 055503 (2010).

41. C.M. Fang, M.A. van Huis, and H.W. Zandbergen, Phys. Rev. B 90, 224108 (2009).

42. C.M. Fang, M.A. van Huis, and H.W. Zandbergen, Scripta Mater.63, 418 (2010).

43. L. J. E. Hofer and E. M. Cohn, Nature (London) 167, 977 (1951).

44. A. Dick, F. Körmann, T. Hickel and J. Neugebauer, Phys. Rev. B84, 125101 (2011).

45. A. F. Guillermet and G. Grimvall, J. Phys. Chem. Solids 53, 105 (1992).

46. P. Olsson, I.A. Abrikosov, L. Vitos and J. Wallenius, J. Nucl. Mater.321, 84 (2003).

47. C. M. Fang, M. H. F. Sluiter, M. A. Van Huis and H. W. Zandbergen, Phys. Rev. B 86, 134114 (2012).

48. C. M. Fang, R. S. Koster, W.-F. Li and M. A. Van Huis, RSC Adv. 4, 7885 (2014).

49. G. Kresse and J. Hafner, Phys. Rev. B47, 558 (1993).

50. G. Kresse and J. Hafner, Phys. Rev. B49, 14251 (1994).

51. G. Kresse and J. Furthmüller, Comput. Mat. Sci.6,15 (1996).

52. P. E. Blöchl, Phys. Rev. B50, 17953 (1994).

53. G. Kresse and J. Furthmüller, Phys. Rev.B54,.1758 (1999).

54. J. P. Perdew, K. Burke K and M. Ernzerhof, Phys. Rev. Lett.77, 3865 (1996).

55. C. Amador, W. R. Lambrecht and B. Segall, Phys. Rev. B46. 1970 (1992).

56. H. J. Monkhorst and J. D. Pack, Phys. Rev. B13. 5188 (1976).

57. G. Rahman, I. G. Kim, H. K. D. Bhadeshia and A. J. Freeman, Phys. Rev. B81, 184423 (2010).

58. H. P. Myers, Introductory Solid State Physics, Taylor and Francis, London/New York / Philadephia (1990).

59. E. Fawcett, Rev. Modern Phys. 60, 209 (1988).

60. R. Hafner, D. Spišák, R. Lorenz and J. Hafner, J. Phys.: Condens. Matter 13, L239 (2001).

61. S. Cottenier, B. De Vries, J. Meersschaut and M. Rots, J. Phys.: Condens. Matter 14, 3275 (2002).

62. N. Sandberg, K. O. E. Henriksson and J. Wallenius, Phys. Rev. B78, 094110(2008).

63. D. J. Branagan, Y. L. Tang, A. V. Sergueeva and A. K. Mukherjee, Nanotechnology 14, 1216 (2003).

64. JANAF Thermochemical Tables, 3rd ed. (Edited by M. W. Chase. C. A. Davies. J. R. Downey, Jr., D. J. Frurip, R. A.McDonald and A. N. Syverud), J. Phys. Chem. Ref. Data 14, Suppl. 1 (1985).

65. C. M. Fang, R. A. de Groot, M. M. J. Bischop and J. Van Kempen, Surf. Sci.445, 123 (2000).

66. T. E. Jones, M. E. Eberhart and D. P. Cloughherty, Phys. Rev. Lett.100, 017208 (2008).

67. R. F. Bader, Atoms in Molecules: A Quantum Theory (Oxford UniversityPress, Oxford, 1990).

68. J. C. Slater, (1964). J. Chem. Phys. 41, 3199 (1964).

69. R. Wyckoff, Crystal Structures, Intersciences, New York (1964).

70. J. G. Wright and J. Goddard, Phil. Mag. 11, 485 (1965).

71. G. A. de Wijs, G. Kresse, L. Vočadlo, D. Dobson, D. Alfè, M. J. Gillan and G. D. Price, Nature (London) 392, 805 (1998).

72. L. Stixrude, R. E. Cohen and D. J. Singh, Phys. Rev. B50, 6442(1994).

73. I. R. Shein, N. I. Medvedeva and A. L. Ivanovskii, Physica B371, 126 (2006).

74. W. F. Bottke, D. Nesvorný, R. E. Grimm, A. Morbidelli and D. P. O'Brien, Nature (London) 439, 821 (2006).

75. U. Herold and U. Köster, Z. Metallk. 69, 326 (1978).

Table 1. Calculated results for α-Fe, α-Cr, and the binary carbides γ-M$_{23}$C$_6$ (M = Cr, Fe and Ni) in comparison with experimental results and previously published calculations.

phase	GGA-PBE (this work)		Previous calculations		Experimental	
	a(Å) /M(μ_B/atom)	ΔE meV/at.	*a* (Å) /M(μ_B/atom)	ΔE meV/at.	*a* (Å) /M(μ_B/atom)	ΔE meV/at.
α-Fe (FM)	*2.831 / 2.21*	-	2.836 [71]/2.17 [71] 2.848 [72]/2.25 [72]		2.861 [69]/2.12 [66]	-
α-Cr (AFM)	*2.837 / 1.07*	-	2.849 [61]/ 0.92 [61] 2.871 [62]/ 1.08 [62]		2.879 [69]/ 0.6 [302]	-
α-Ni (FM)	*3.524 / 0.63*	-	3.517 [73]/ 0.63 [73]		3.518 [69]/0.60 [47]	-
γ-Cr$_{23}$C$_6$ (NM)	10.531 /-	-96.7	10.903 [11] 10.53 [31] 10.31 [31]	~ -95 [31] ~ -85 [32]	10.66 [1] 10.64 [23]	*~ -82* [38,45]
γ-Fe$_{23}$C$_6$ (FM)	10.467 / 2.04	*+19.5*	*10.627* [12] */ -* *10.4668* /2.04 [13,39]	~ +45 [39]	10.639 [63] / -	~ +36 [38,45]
γ-Ni$_{23}$C$_6$ (FM)	10.367 / 0.06	+118.7	*-*		*-*	~ +63 [38,45]

Table 2. Calculated results (electronic configurations, local magnetic moments in the atomic spheres, as well as interatomic distances in binary γ-$M_{23}C_6$ (M = Cr, Fe and Ni).

Atom	Site	γ-$Cr_{23}C_6$ (NM) Bonds (Å)	M (μ_B)	γ-$Fe_{23}C_6$ (FM) Bonds (Å)	M (μ_B)	γ-$Ni_{23}C_6$ (FM) Bonds (Å)	M (μ_B)
M1	4a	Cr1-Cr4: 2.53(×12) Cr1:$4s^{0.48}4p^{0.57}3d^{4.39}$	0.00	Fe1-Fe4: 2.51(×12) Fe1:$4s^{0.52}4p^{0.60}3d^{6.40}$	2.53	Ni1-Ni3: 2.38(×4) Ni1:$4s^{0.52}4p^{0.59}3d^{8.58}$	0.06
M2	8c	Cr2-Cr3: 2.39(×4) Cr2:$4s^{0.43}4p^{0.51}3d^{4.30}$	0.00	Fe2-Fe3: 2.43(×4) Fe2:$4s^{0.46}4p^{0.52}3d^{6.30}$	2.82	Ni2-Ni3: 2.39(×4) Ni2:$4s^{0.48}4p^{0.48}3d^{8.47}$	0.40
M3	32f	Cr3-Cr2: 2.39 -Cr3: 2.51(×3) -Cr4: 2.61(×6) -C: 2.09(×3) Cr3:$4s^{0.46}4p^{0.69}3d^{4.50}$	0.00	Fe3-Fe2: 2.43 -Fe3: 2.43(×3) -Fe4: 2.61(×6) -C: 2.05(×3) Fe3:$4s^{0.51}4p^{0.75}3d^{6.65}$	1.78	Ni3-Ni2: 2.39 -Ni3: 2.51(×3) -Ni4: 2.61(×6) -C: 2.09(×3) Ni3:$4s^{0.54}4p^{0.76}3d^{8.62}$	0.04
M4	48h	Cr4-Cr1: 2.53 -Cr3: 2.61(×4) -Cr4: 2.38,2.53(×4) -C: 2.11(×2) Cr4:$4s^{0.46}4p^{0.65}3d^{4.45}$	0.00	Fe4-Fe1: 2.51 -Fe3: 2.61(×4) -Fe4: 2.38,2.51(×4) -C: 2.10(×2) Fe4:$4s^{0.50}4p^{0.69}3d^{6.45}$	2.15	Ni4-Ni1: 2.53 -Ni3: 2.61(×4) -Ni4: 2.38,2.53(×4) -C: 2.11(×2) Ni4:$4s^{0.54}4p^{0.72}3d^{8.66}$	0.01
C	24e	C-Cr3: 2.09(×4) -Cr4: 2.11(×4) C:$2s^{1.13}2p^{2.09}3d^{0.07}$	0.00	C-Fe3: 2.05(×4) -Fe4: 2.10(×4) C:$2s^{1.12}2p^{2.01}3d^{0.08}$	-0.15	C-Ni3: 2.09(×4) -Ni4: 2.11(×4) C: $2s^{1.12}2p^{1.94}3d^{0.08}$	0.00

Table 3 Calculated formation energies (meV/atom) for γ-$M_{22}XC_6$, whereby one M atom in γ-$M_{23}C_6$ at the M1, M2, M3, or M4 site is replaced by another 3d transition metal X.

X at site	γ-$Ni_{22}FeC_6$ ΔE(meV/at.) /M(μ_B/Fe)	γ-$Fe_{22}NiC_6$ ΔE(meV/at.) /M(μ_B/Ni)	γ-$Cr_{22}FeC_6$ ΔE(meV/at.) (NM)	γ-$Fe_{22}CrC_6$ ΔE(meV/at.) /M(μ_B/Cr)
M1	+114.5 /2.94	+5.0 /0.72	-114.7	+4.2 /-2.37
M2	+107.3 /3.21	+68.8 /0.86	-83.2	+15.5 /-2.19 (AF to Fe)
M3	+114.7 /1.80	+28.5 /0.35	-87.5	+20.0 /-0.41 (AF to Fe)
M4	+116.8 /2.50	+24.1 /0.49	-90.9	+18.1 /-1.36 (AF to Fe)

Table 4. Calculated lattice parameters and formation energies for $(Fe,Cr)_{23}C_6$ phases using the DFT-GGA approach. The results are also displayed in Figure 3. The energies of phases with a negative formation enthalpy are printed boldface.

Formula		a (Å) (experimental)	$\Delta E1$ (meV/atom)
$Cr_{23}C_6$	Cr: 4a, 8c, 32f, 48h	10.528 (10.650 [23]) 10.903 [11,12] 10.34 [31], 10.53 [31]	*-96.7* *~-100.* [31]
$Cr_{22}Fe_1C_6$	Fe: 4a Cr: 8c, 32f, 48h	10.517	*-114.7*
$Cr_{21}Fe_2C_6$	Fe 8c Cr: 4a, 32f, 48h	10.507	*-0.8*
$Cr_{20}Fe_3C_6$	Fe: 4a, 8c Cr: 32f,48h	10.496	*-87.1*
$Cr_{15}Fe_8C_6$	Fe: 32f Cr: 4a, 8c, 48h	10.403	*-29.0*
$Cr_{14}Fe_9C_6$	Fe: 4a, 32f Cr: 8c, 48h	10.398	*-41.3*
$Cr_{13}Fe_{10}C_6$	Fe: 8c, 32f Cr: 4a, 48h	10.412	+2.5
$Cr_{12}Fe_{11}C_6$	Fe: 4a, 8c, 32f Cr: 48h	10.376	*-1.3*
$Cr_{11}Fe_{12}C_6$	Fe: 48h Cr: 4a, 8c, 32f	10.387	+3.9
$Cr_{10}Fe_{13}C_6$	Fe: 4a, 48h Cr: 8c, 32f	10.442	-36.2
$Cr_9Fe_{14}C_6$	Fe: 8c, 48h Cr: 4a, 32f	10.465	*-33.5*
$Cr_8Fe_{15}C_6$	Fe: 4a, 8c, 48h Cr: 32f	10.445	*-6.7*
$Cr_3Fe_{20}C_6$	Fe: 32f, 48h Cr: 4a,8c	10.411	+5.3
$Cr_2Fe_{21}C_6$	Fe: 4a, 32f, 48h Cr: 8c	10.391	+21.8
$Cr_1Fe_{22}C_6$	Fe: 8c,, 32f, 48h Cr: 4a	10.452	+4.2
$Fe_{23}C_6$	Fe: 4a,8c,32f, 48h	10.467(10.639 [63])	+19.5
$Cr_{22}C_6$	Cr: 8c, 32f,48h	10.482	*-83.3*
$Fe_{22}C_6$	Fe: 8c, 32f,48h	10.414	+33.5

Figure captions

Figure 1. Schematic crystal structure of the γ-$M_{23}C_6$ phase (M=Cr, Ni, Fe). The rose spheres represent the M1 atoms at the 4a sites, purple spheres M2 atoms at the 8c sites, red spheres M3 atoms at the 32f sites, and dark-red spheres M4 atoms at the 48f sites; the dark spheres represent C atoms at the 24e sites. For simplicity, only M-C bonds are shown.

Figure 2. The relationship between the atomic volumes as determined using the Bader approach, [67] and the local magnetic moments for γ-$Fe_{23}C_6$.

Figure 3. Formation energies (top) and lattice parameters (bottom) for γ-$(Fe,Ni)_{23}C_6$ and γ-$(Fe,Cr)_{23}C_6$ phases as a function of Fe concentration {$X(Fe) = n(Fe)/[n(Fe) + n(M)]$}. In (a), the solid circles represent the results for the Fe-Ni phases, solid squares results for the Fe-Cr phases. Lines are drawn to guide the eye.

Figure 4. Local magnetic moments for γ-$(Fe,Ni)_{23}C_6$ (top) and γ-$(Fe,Cr)_{23}C_6$ (bottom) as a function of Fe concentration {$X(Fe) = n(Fe)/[n(Fe) + n(M)]$}. The circles represent the magnetic moments at the M1 atoms, solid squares at the M2 atoms, solid triangles-up at the M3 atoms and solid triangle-down at the M4 atoms. The black curves are for the Ni or Cr atoms and the red curves are for the Fe atoms. Lines are drawn to guide the eye.
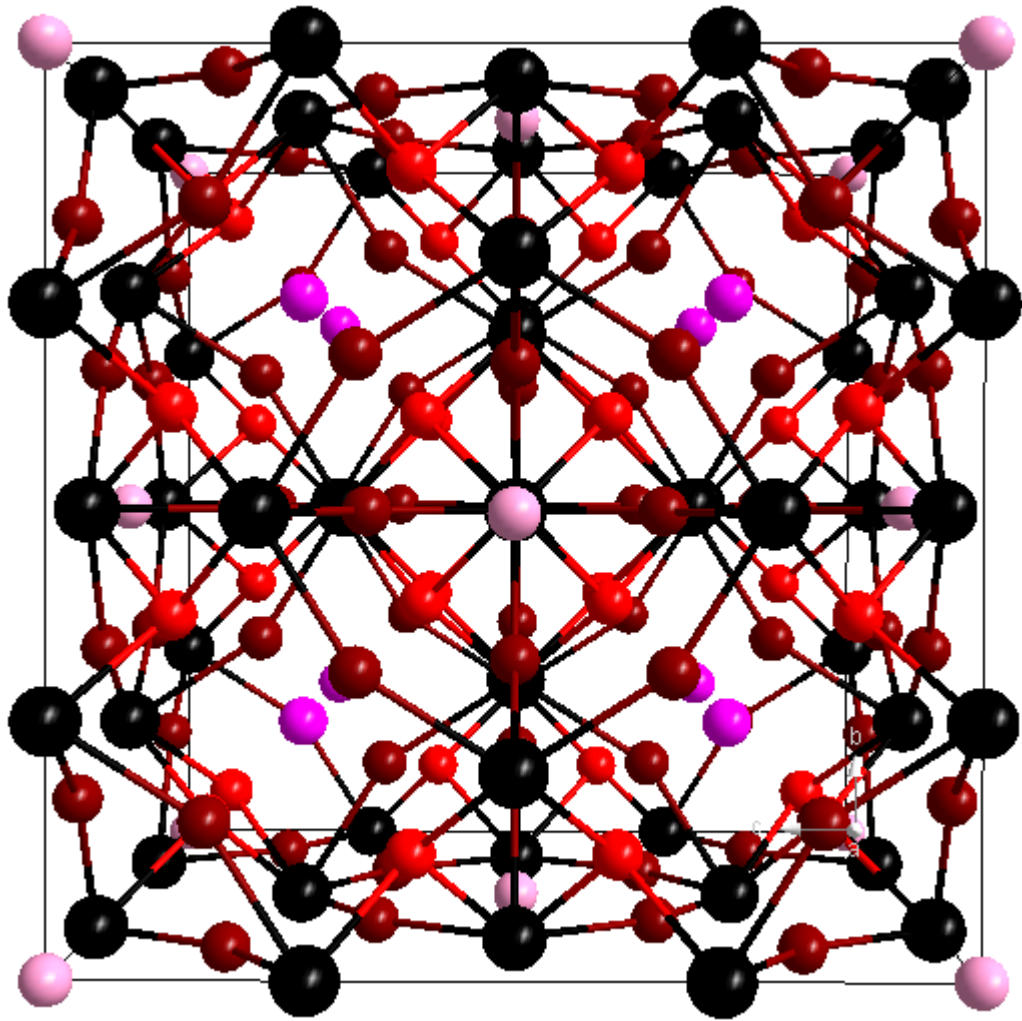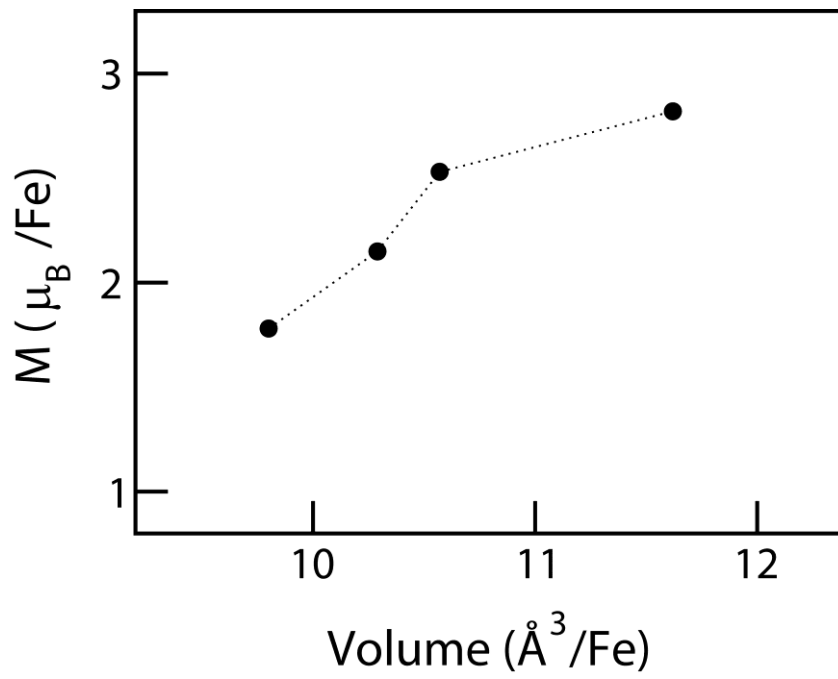
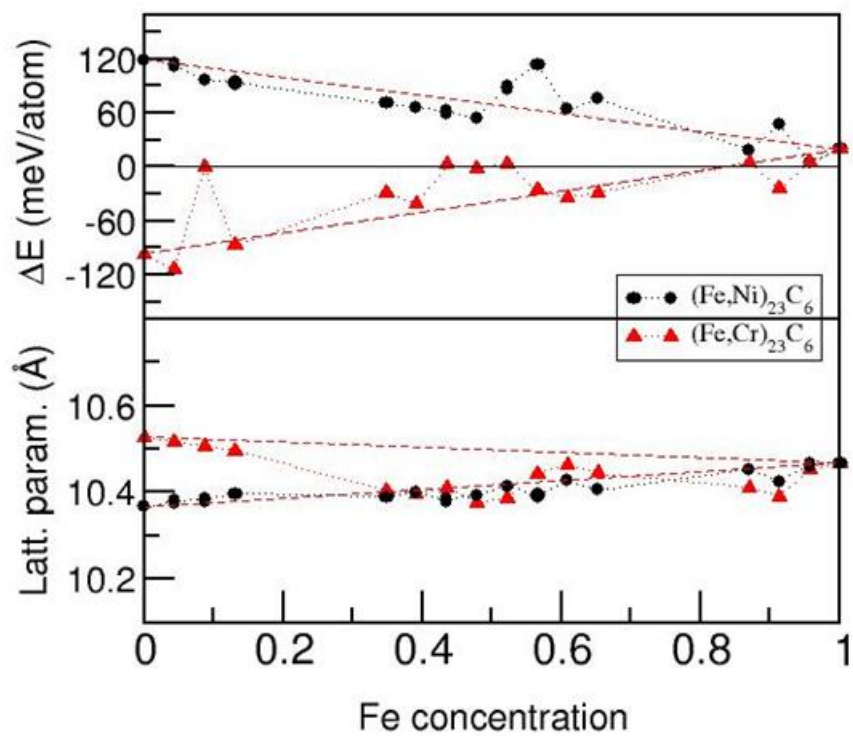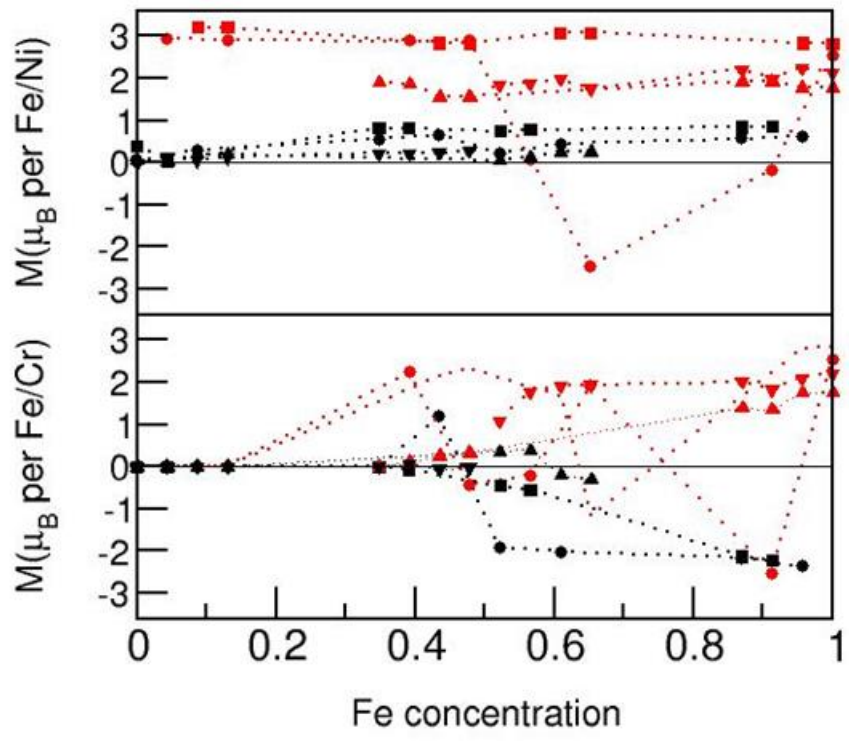Fig. 1. (Fang, *et al*.)

Fig. 2 (Fang, *et al.*)

Fig. 3 (Fang, *et al.*)

Fig. 4 (Fang, *et al*.)